Snapshotting the Excited-State Planarization of Chemically Locked *N,N'*-Disubstituted Dihydrodibenzo[*a,c*]phenazines

Wei Chen,[†,§] Chi-Lin Chen,[‡,§] Zhiyun Zhang,[†,‡,§] Yi-An Chen,[‡] Wei-Chih Chao,[‡] Jianhua Su,[†] He Tian,*,[†] and Pi-Tai Chou*,[‡]

[†]Key Laboratory for Advanced Materials and Institute of Fine Chemicals, East China University of Science & Technology, Shanghai 200237, P. R. China

[‡]Department of Chemistry, National Taiwan University, Taipei, 10617 Taiwan, R.O.C.

🅢 *Supporting Information*

ABSTRACT: For deeper understanding of the coupling of electronic processes with conformational motions, we exploit a tailored strategy to harness the excited-state planarization of *N,N'*-disubstituted dihydrodibenzo[*a,c*]phenazines by halting the structural evolution via a macrocyclization process. In this new approach, 9,14-diphenyl-9,14-dihydrodibenzo[*a,c*]phenazine (**DPAC**) is used as a prototype, in which the *para* sites of 9,14-diphenyl are systematically enclosed by a dialkoxybenzene-alkyl-ester or -ether linkage with different chain lengths, imposing various degrees of constraint to impede the structural deformation. Accordingly, a series of **DPAC-*n*** (*n* = 1−8) derivatives were synthesized, in which *n* correlates with the alkyl length, such that the strength of the spatial constraint decreases as *n* increases. The structures of **DPAC-1**, **DPAC-3**, **DPAC-4**, and **DPAC-8** were identified by the X-ray crystal analysis. As a result, despite nearly identical absorption spectra (onset ∼400 nm) for **DPAC-1−8**, drastic chain-length dependent emission is observed, spanning from blue (*n* = 1, 2, ∼400 nm) and blue-green (*n* = 3−5, 500−550 nm) to green-orange (*n* = 6) and red (*n* = 7, 8, ∼610 nm) in various regular solvents. Comprehensive spectroscopic and dynamic studies, together with a computational approach, rationalized the associated excited-state structure responding to emission origin. Severing the linkage for **DPAC-5** via lipase treatment releases the structural freedom and hence results in drastic changes of emission from blue-green (490 nm) to red (625 nm), showing the brightening prospect of these chemically locked **DPAC-*n*** in both fundamental studies and applications.
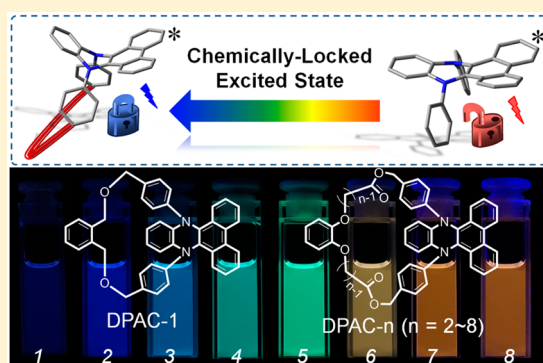
1. INTRODUCTION

Recently, specific fluorophores with anomalous electronically excited-state phenomena, giving rise to, e.g., large Stokes shift or multicolor emission, have drawn considerable attention because of their exploitations in flexible full-color displays and biosensors.[1] To facilitate the rational design of applicable molecules with intriguing photophysical properties, a great deal of in-depth studies along with the excited-state dynamics of the fluorophores have been conducted, among which excited-state electron transfer,[2−4] proton transfer,[5] and energy transfer[6] are three essential processes.
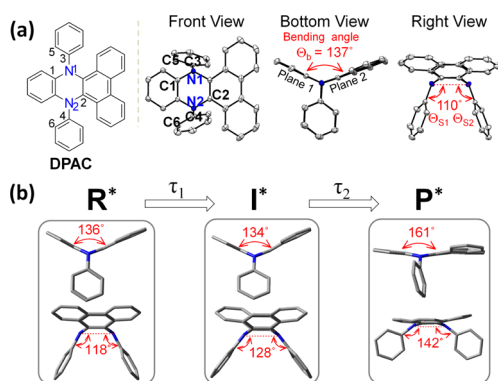
Beyond the three processes described above, the coupling of nuclear motions with electronic processes is also one of the most fundamental issues in chemistry. Whereas the intramolecular rotations (or twisting) coupled with electron transfer have been extensively studied,[2,3] rare cases are those chromophores demonstrating elongation of the π-delocalization due to bent-to-planar motions, modulating dramatically the luminescence.[7] In this regard, our attention was attracted by a series of hole transporting materials, *N,N'*-disubstituted dihydrodibenzo[*a,c*]phenazines (DHPs). We discovered the unusual photophysical property that some DHPs reveal

anomalously large Stokes-shifted emission in regular solvents.[8] Using 9,14-diphenyl-9,14-dihydrodibenzo[*a,c*]phenazine (**DPAC**, see Figure 1a) as a prototype, we found that, upon excitation at the lowest lying absorption band at ∼350 nm, **DPAC** exhibits a ∼610 nm red emission that is independent of the solvent polarity. The spectroscopic and dynamic results lead us to propose a mechanism of skeletal motion toward the planarization coupled with the elongation of the π-delocalization over the benzo[*a,c*]phenazines moiety. Along the planarization, **DPAC** also encounters the steric hindrance raised by the bulky *N,N'*-disubstitutes, leading to a local minimum state, which then further relaxes to maximize the planarization. The overall structural relaxation process of **DPAC** can be qualitatively described by a sequential kinetic pattern depicted in Figure 1b below.[8a]

As a result, at the early time domain (a few to a few tens of picoseconds) after Franck−Condon excitation, the temporal evolution of the emission of **DPAC** in the regular organic solvents reveals time dependent panchromatic emission,

© 2017 American Chemical Society   **1636**   DOI: 10.1021/jacs.6b11789
J. Am. Chem. Soc. 2017, 139, 1636−1644

Figure 1. (a) Chemical structure of DPAC as well as its crystal structure from front, bottom, and right views with the selected angles: $\Theta_b = \angle C1-N1-N2-C2$, $\Theta_{S1} = \angle C3-N1-N2$, and $\Theta_{S2} = \angle C4-N2-N1$. (b) The structural relaxation of DAPC and its derivatives in the electronically excited state. Using DAPC as the prototype, R* specifies the initially prepared state, and I* is an intermediate with the local minimum energy, both of which possess a certain charge transfer character. P* denotes the final planarization state with the global minimum energy along the structural relaxation process. R*, I*, and P* are all assumed to be the emissive states. The DFT optimized geometries of DPAC in R*, I*, and P* states are depicted. Note the difference in Θ_b and $\Theta_{S1, S2}$ among R*, I*, and P*.

consisting of initial charge transfer (R*), intermediate (I*), and the planarized, global minimized emission (P*), which is drastically different from that of the solely red emission (P*) observed in the room-temperature steady-state approach. The dynamics of structural relaxation of DHPs were affected by the steric hindrance raised by N,N′-disubstituted side chain motion. That is, the more steric hindrance induced by the bulky side chain may cause further retardation of structural relaxation along the planarization. This suggests the feasibility of "controlling" the planarization process through constraining the N,N′-disubstituted side chain motion.

Aiming to understand deeply the coupling of excited-state electronic processes with conformational motions, we thus conceived a series of annulated structures based on **DPAC** as a core, where *para* sites of the 9,14-diphenyl moieties are chemically threaded by dialkoxybenzene-alkyl-ester (or -ether) with different chain lengths, forming a series of new DHPs, **DPAC-n** (n = 1–8, see Scheme 1). Our aim was to impose various degrees of constraint to impede the excited-state structural deformation in hope of trapping a specific conformation so that we would be able to take a snapshot of the structural evolution and the associated photoluminescence. As elaborated in the following sections, the proof of concept is rendered by the constraint dependent spectral evolution of **DPAC-n** spanning much of the panchromatic region. We also demonstrate that scissoring the linkage leads to structural relaxation and consequently drastic changes of the emission property, demonstrating their fruitful potential in molecular sensing.

2. RESULTS AND DISCUSSION

2.1. Design, Synthesis, and Crystal Structures.
A series of **DPAC-n** derivatives (n = 1–8, see Scheme 1), where n correlates with the different alkyl lengths, were synthesized and characterized. In a qualitative manner, we expected a decrease in constraint strength upon increasing n. As depicted in Scheme 1, treatment of **DPAC** with Vilsmeier reagent introduced two

Scheme 1. Synthetic Route and Chemical Structures of Chemically Locked 9,14-Diphenyl-9,14-dihydrodibenzo[a,c]phenazines DPAC-n[a]
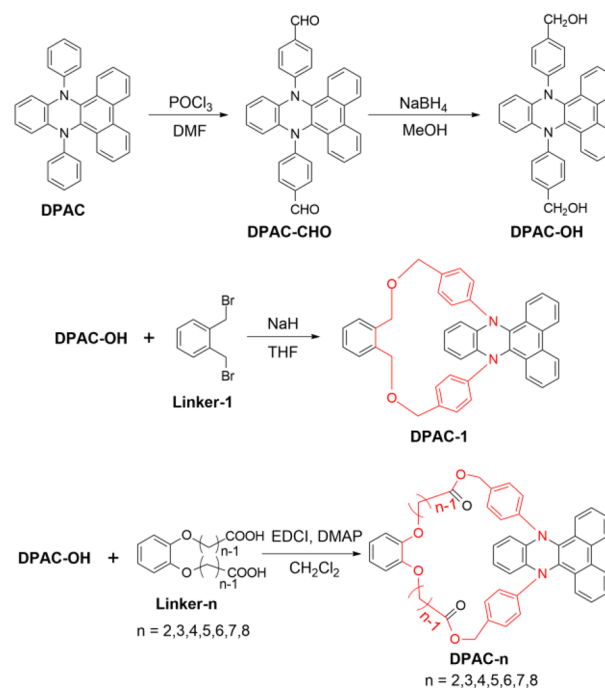
[a]EDCI: 1-ethyl-3-(3-(dimethylamino)propyl)carbodiimidehydrochloride. DMAP: 4-dimethylaminopyridine.

aldehyde groups in the *para* sites of 9,14-diphenyl of **DPAC** and gave the dialdehyde **DPAC-CHO**, which was subsequently reduced by sodium borohydride to give the key intermediate dibenzyl alcohol **DPAC-OH**, a structure that could be further cyclized by a dialkoxybenzene-alkyl-ether or -ester linkage with different chain lengths. Therefore, diol **DPAC-OH** reacted with **Linker-1** 1,2-bisbromomethylbenzen (NaH, THF, reflux) to deliver the smallest macrocycle **DPAC-1** in this work. To tune the chain length, a series of compounds, **Linker-n** (n = 2–8, see Scheme 1), end-capped with two carboxyl groups were prepared by nucleophilic substitution of 1,2-benzenediol with bromo-alkyl acids bearing different alkyl chain lengths (see Scheme S1 in the Supporting Information (SI)). Finally, various macrocycles **DPAC-n** (n = 2–8) were obtained from esterification of diol **DPAC-OH** with **Linker-n** (n = 2–8) using EDCI/DMAP (see Scheme 1). Furthermore, the molecular structures of **DPAC-n** (n = 1, 3, 4, and 8) were further confirmed by single-crystal X-ray diffraction analysis.

By slow evaporation from dichloromethane/ethanol mixture solutions, we were able to grow single crystals of **DPAC-n** (n = 1, 3, 4, and 8). As shown in Figure 2, all corresponding X-ray structures reveal significant nonplanar distortions inherited from **DPAC**. For the convenience of analysis, three angles (Θ_b, Θ_{S1}, and Θ_{S2}) in the single-crystal structures were put forward and calculated. Using **DPAC** for illustration (see Figure 1a), Θ_b ($\angle C1-N1-N2-C2$) represents the bending angle between planes 1 (C1, N1, and N2) and 2 (N1, N2, and C2), while the angle between axes N1–N2 and N1–C3 or N2–C4 is denoted as Θ_{S1} ($\angle C3-N1-N2$) or Θ_{S2} ($\angle C4-N2-N1$). As a result, Θ_b of 134° for **DPAC-1** signifies the sharp decrease of the bent angle compared with those of **DPAC-3**, **-4**, and **-8** (138–143°). In comparison to the Θ_b of ~137° for **DPAC**, a decrease of up to ~5° in Θ_b for **DPAC-1** may signify its further nonplanar
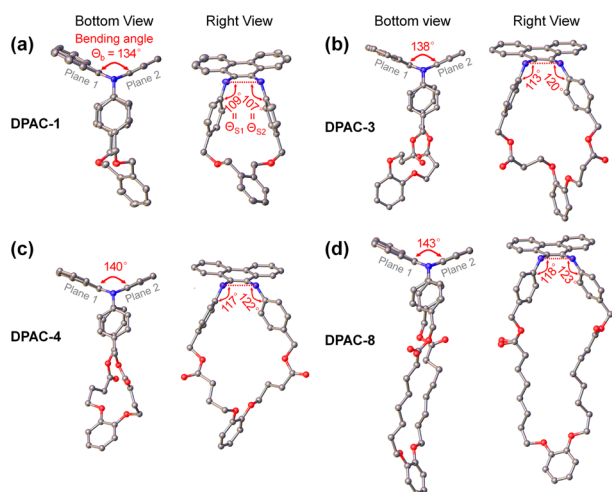
Figure 2. Single-crystal structures of (a) **DPAC-1**, (b) **DPAC-3**, (c) **DPAC-4**, and (d) **DPAC-8** from their two angles of view with the values of Θ_b, Θ_{S1}, and Θ_{S2}.

distortion upon imposing the small alkyl chain constraint (vide infra). Meanwhile, Θ_{S1} and Θ_{S2} obviously rise from ~109° to ~118° and ~107° to ~123°, respectively. Note that, in contrast to **DPAC**, the Θ_{S1} of which is in close proximity to Θ_{S2}, there is an obvious disparity between Θ_{S1} and Θ_{S2} in **DPAC-3**, **-4**, and **-8**, which might be attributed to the flexible chain motion. Theoretically, upon electronic excitation of N,N'-disubstituted dihydrodibenzo[a,c]phenazines, a favorable bent-to-planar motion takes place to elongate the π-conjugation. In this sense, conformational information derived from single-crystal analysis is consistent with the explanation, as structural strain decreases upon increase of the length of the alkyl chain.

2.2. Steady-State Photophysical Properties. The normalized absorption and emission spectra of **DPAC-n** ($n = 1−8$) in various solvents from nonpolar cyclohexane to highly polar acetonitrile are shown in Figure 3 and Figure S1 (absorption in different solvents). The absorption peak wavelengths of 345−350 nm (onset at ~400 nm) for **DPAC-2−8** in various studied solvents are about the same as that of **DPAC** (see Figure 3i). In comparison, distinctly, both the absorption onset (~385 nm) and peak wavelength (~340 nm) of **DPAC-1** are slightly blue-shifted by ~5−15 nm. On one hand, this result indicates that **DPAC-2−8** have a core chromophore similar to that of the constraint-free **DPAC** in the ground state. On the other hand, it also affirms the above structural analyses of a more crooked structure for **DPAC-1** (cf., **DPAC-2−8**), probably due to its tight structure constraint (vide supra, see Figure 2), rendering less π-delocalization.

Despite the similarity in absorption spectra, **DPAC-n** species exhibit remarkable differences in the emission properties. For **DPAC-1** and **DPAC-2**, the peak wavelength of fluorescence is located at 400 and 420 nm, respectively, in toluene (Figure 3a,b), followed by a trend of red-shifted emission of **DPAC-3** (460 nm), **DPAC-4** (478 nm), **DPAC-5** (492 nm), **DPAC-6** (590 nm), **DPAC-7** (600 nm), and **DPAC-8** (607 nm) (Figure 3c−h). Accordingly, the emission peak wavelength is distinctly chain-length (i.e., n) dependent, being red-shifted upon increasing n from **1** to **8**. Corresponding to emission spectra, fluorescence images of **DPAC-n** ($n = 1−8$) clearly exhibit the red shift of emission with increment of chain-length (see Figure 4). From **DPAC-1** to **DPAC-8** in toluene, the emission color changes in an order of violet-blue (0.16, 0.03), palatinate blue
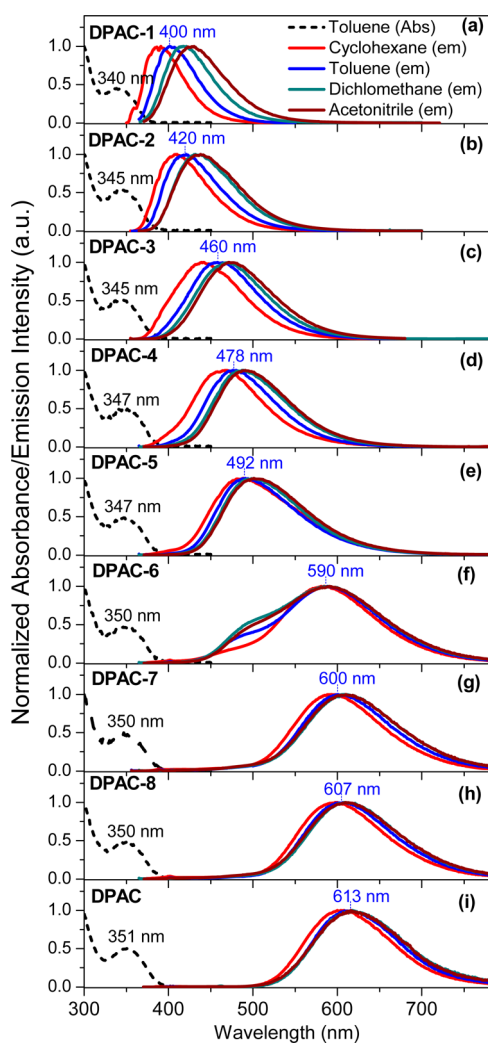
Figure 3. Steady-state absorption (in toluene, dashed line) and photoluminescence (solid line) spectra of (a−h) **DPAC-1−8** and (i) **DPAC** in various solvents at room temperature ($\lambda_{ex} = 360$ nm).
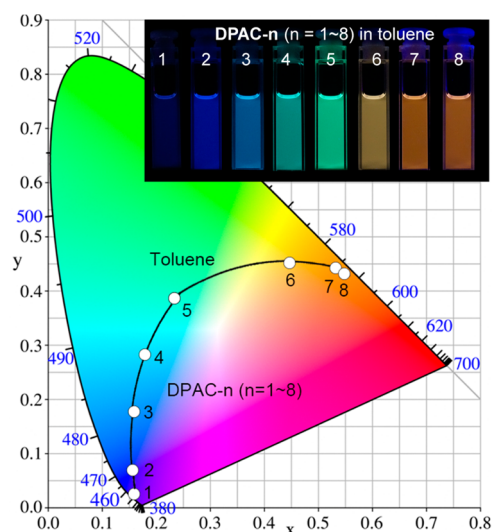
Figure 4. Chromaticity coordinates (CIE) of **DPAC-n** ($n = 1−8$) in toluene at room temperature ($\lambda_{ex} = 360$ nm). Insert: the fluorescence images of **DPAC-n** ($n = 1−8$) in toluene under irradiation of 365 nm UV light.

(0.15, 0.07), maya blue (0.16, 0.18), turquoise (0.18, 0.28), aquamarine (0.23, 0.39), yellow (0.45, 0.45), orange (0.53, 0.44), and dark orange (0.55, 0.44). Apparently, the drastic chain-length dependent emission spans much of the visible range. For **DPAC-6**, in addition to the 590 nm emission, there appears to be another emission band maximized at ~490 nm, showing dual or even multiple emission properties. Careful analysis also indicates that the blue and green emission for **DPAC-1−5** is dependent on solvent polarity, being red-shifted as much as ~40 nm in peak wavelength from cyclohexane to acetonitrile (Figure 3a−e), whereas the red emission for **DPAC-6−8** is only slightly dependent on solvent polarity (Figure 3f−h). This is also well-demonstrated by the fluorescence images of **DPAC-n** (n = 1−8) in various solvents (see Figure S2). For **DPAC-4**, for example, with the solvent polarity increasing from nonpolar cyclohexane to highly polar acetonitrile, the emission color tunes from blue (0.17, 0.21) to green (0.21, 0.38), exhibiting remarkable solvatochromism. The results manifest the difference in the transition characters of these n dependent, multiple color emissions with conformational motions.

It has been established that the nonplanar, V-shaped **DPAC** and its derivatives undergo structural bending motion between plane 1 and plane 2, i.e., along Θ_b (see Figure 1b) in the electronically excited state, reaching a more planar configuration to extend the π-conjugation and hence an energy minimum.[8a] The bending process along Θ_b is accompanied by the simultaneous optimization of Θ_{S1} and Θ_{S2} and hence encounters the steric hindrance introduced by the N,N′-disubstituted side chains, which may evolve to a local minimum energy. As for the local minimum states, the nonplanar structure may localize the N,N′-disubstituents and dibenzo-[a,c]phenazine moieties such that the transition possesses charge transfer character. Thus, previous time-resolved measurement was able to acquire various transient emissions at different time domains ascribed to initial charge transfer (R*), and intermediate (I*) and planarization (P*) emission (see Figure 1b).

In this study, via inserting an alkyl chain to impose the strain energy and halt the planarization midway, we were able to resolve different statuses of the structural evolution of the **DPAC** core chromophore even in a steady-state manner, which is tentatively attributed to the initially prepared state emission (400−420 nm, **DPAC-1** and **DPAC-2**), the intermediate emission (460−520 nm, **DPAC-3−5**), and the planarization emission (600−620 nm, **DPAC-7** and **DPAC-8**). Despite the solvent's independent absorption spectra, the short-wavelength emission bands (400−520 nm) are red-shifted significantly upon increasing the solvent polarity, indicating their excited-state charge transfer property and hence the occurrence of solvatochromism. Conversely, the red emission band originating from planarized structure is much less subject to solvent polarity, confirming its delocalized ππ* character.

To better understand the solvatochromism for short-wavelength emissions of **DPAC-1−6**, the solvent effect on the emission properties can be further described by the Lippert−Mataga equation, which is expressed as

$$\Delta\nu = \nu_{abs} - \nu_{em} = 2\Delta\mu^2\Delta f / (hca^3) + \text{constant}$$

Here, the following abbreviations are used: $\Delta\nu$ denotes the Stokes shift, ν_{abs} and ν_{em} correspond to the absorption and the emission maxima in terms of wavenumbers $(cm)^{-1}$, respectively, $\Delta\mu$ is the change of dipole moment between ground and

excited states, h is Planck's constant, c is the speed of light, Δf is the orientational polarizability of the solvent, and a is the Onsager solvent cavity radius which is obtained by B3LYP/6-31+g(d,p) method in this study, assuming a spherical shape of the molecule. Figure S3 showcases the Lippert−Mataga plots of **DPAC-1−6**, and $\Delta\mu$ is then calculated from the slope of the Lippert−Mataga plots and listed in Table S1. The deduced $\Delta\mu$ values for **DPAC-1−6** in short-wavelength emission bands are large (>7.7 D), indicating that the R* and I* have a much larger dipolar moment than their corresponding ground states, confirming their excited-state charge transfer character. We also found that the $\Delta\mu$ values for **DPAC-1−6** decrease upon increase of the length of the alkyl chain, due perhaps to the released constraint via the longer alkyl-ester linkage. Later, we will elaborate that the intermediate corresponds to the skeleton motion of the side chain without significant planarization.

Upon planarization, the emission is dominated by the ππ* delocalized transition of the dibenzo[a,c]phenazine moiety, which has a negligible charge transfer character. Interestingly, **DPAC-6** in the excited state reaches a critical stage where the intermediate emission decay rate is competitive with its rate of planarization, resulting in both intermediate and planarization emissions. This viewpoint is firmly supported in the later time-resolved approach. Finally, independent of **DPAC-1−8**, normal Stokes-shifted blue (~400−430 nm) emission was observed for all titled compounds in the solid (see Figure S4). The result firmly supports that the planarization process of **DPAC-1−8** required large-amplitude structural deformation, which is prohibited in the solid due to the lattice constraint.

2.3. Time-Resolved Emission Spectroscopy.

To gain in-depth insight into the underlying relaxation mechanism, we then further performed time-resolved measurements. Two representative compounds, **DPAC-5** and **DPAC-6**, will receive particular focus. **DPAC-6** is of prime concern due to its obvious two emissions maximized at 490 and 590 nm, which possibly originate from intermediate and planarization emission, respectively. **DPAC-5** is selected as the other prototype because it has a proximal alkyl chain length with respect to **DPAC-6** but exhibits a very different emission spectrum.

As for **DPAC-5**, we first carried out a femtosecond fluorescence up-conversion study in toluene to probe the reaction dynamics in the early time domain. The results are shown in Figure 5a, and pertinent data are listed in Table 1. Upon 370 nm excitation and monitoring at the blue side of the emission (450 nm), the relaxation dynamics for **DPAC-5** exhibited an instant rise (<system response of 120 fs), followed by a very fast decay component of 23 ± 2 ps decay components. Upon monitoring at 500, 550, 600, and 650 nm, shown in Figure 5a, a finite rise component (negative pre-exponential value) gradually appeared, which was fitted to be within 23 ± 2 ps. Also, independent of the monitored emission wavelength, there existed a very long population decay component that could not be completely acquired by the up-conversion technique. Alternatively, the long population decay kinetics were resolved by the pico-nanosecond time correlated single photon counting (TCSPC) measurement. The results depicted in Figure 5b reveal a single exponential decay component of 10.2 ns for all monitored emission wavelengths, indicating only a single population decay component.
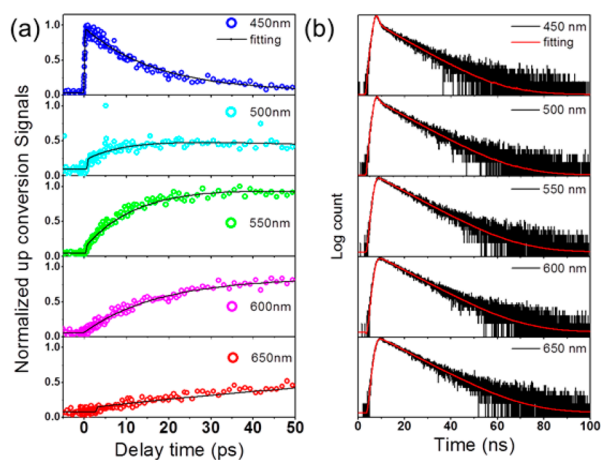
In comparison to those of **DPAC-5**, much different relaxation dynamics were resolved for **DPAC-6**. Figure 6a reveals the early relaxation dynamics for **DPAC-6** in toluene, and pertinent fitted data are listed in Table 1. The relaxation
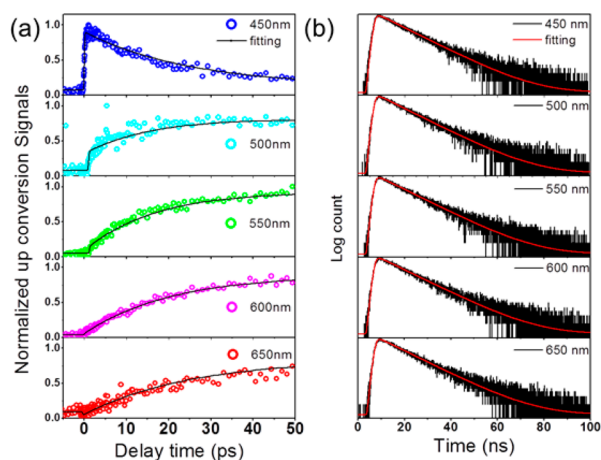
Figure 5. (a) Femtosecond and (b) nanosecond fluorescence transients of **DPAC-5** in toluene at room temperature observed at various wavelengths as depicted. See Table 1 for the fitting results (λ_{ex} = 370 nm). Note: For clarity, a logarithm plot is used in part b.

Figure 6. (a) Femtosecond and (b) nanosecond fluorescence transients of **DPAC-6** in toluene at room temperature observed at various wavelengths as depicted. See Table 1 for the fitting results (λ_{ex} = 370 nm). Note: A logarithm plot is used in part b for clarity to show biexponential decay for 450 and 500 nm emissions.

dynamics at the blue edge of emission (450 nm) consisted of an instant rise (<120 fs), followed by a fast decay of 17 ps and a rather small amplitude, but a much longer-lived component that remained constant at the acquisition range of 50 ps. This long decay component was further probed by the nanosecond TCSPC. The result shown in Figure 6b (uppermost) revealed biexponential decay behavior with time constants fitted to be 0.33 and ~9 ns.

Upon increasing the monitored emission wavelengths to 500 and 550 nm, as shown in Figure 6a for femtosecond up-conversion data, the early 17 ps decay component observed at 450 nm disappeared and became a 17 ps rise component. Note that in Figure 6a (for 500 and 550 nm) the partial overlap between 17 ps rise and 17 ps decay components canceled out, giving an instant rise component. Also, the long decay component increased the weighting ratio (% in pre-exponential factor) from 500 to 550 nm. The results of corresponding nanosecond TCSPC (see Figure 6b) also clearly indicated that the 0.33 ns decay component reduced its weighting ratio from 500 to 550 nm, which correlated with the appearance of a long rise component shown in the up-conversion study (see Figure 6b and Table 1). With an extension of the monitored wavelength to 650 nm, as shown in the TCSPC results (Figure 6b, lowermost), the 0.33 ns decay component was not resolvable anymore. Instead, a 0.33 ns rise component was resolved, followed by a ~9 ns population decay. This 0.33 ns

long rise component can be seen from the up-conversion study as well (Figure 6a, lowermost), although the fluorescence up-converted data could not be precisely fitted due to the small acquisition time range of 50 ps.

The above time-resolved measurements clearly support the concept that the degree of excited-state planarization of **DPAC** can be controlled by chemically imposing an alkyl chain to act as a brake. As shown in Scheme 2, upon excitation at the lowest lying state (S_1), **DPAC-5** undergoes a structural relaxation process from the initially prepared state (R^*) to an intermediate (I^*), i.e., $R^* \rightarrow I^*$ with a time constant of 23 ± 2 ps. The intermediate I^* is then subject to the strength imposed by the $n = 5$ alkyl chain, such that further structural evolution is prohibited, resulting in a long population decay time of 10.2 ns. For **DPAC-6**, we reasonably assign the time constants of the $R^* \rightarrow I^*$ and $I^* \rightarrow P^*$ processes to be 17 ps (τ_1) and 0.33 ns (τ_2), respectively, followed by a population decay of the P^* state of ~9 ns (τ_P). Clearly, the $R^* \rightarrow I^*$ processes for **DPAC-5** (24 ps) and **DPAC-6** (17 ps) are longer than that of **DPAC** (2.8 ps, τ_1),[8a] manifesting that the dialkoxybenzene-alkyl-ester linkages $n = 5$ (**DPAC-5**) and $n = 6$ (**DPAC-6**) increase the strain during the $R^* \rightarrow I^*$ process. The increase in n releases strain and hence results in a faster $R^* \rightarrow I^*$ process for **DPAC-6** than that for **DPAC-5**. The prohibition of the $I^* \rightarrow P^*$ process for **DPAC-5** implies that the $I^* \rightarrow P^*$

Table 1. Fitting Results of TCSPC and Femtosecond Fluorescence Up-Conversion Measurements for DPAC-5 and DPAC-6 in Toluene at Room Temperature

	DPAC-5		DPAC-6	
λ_{probe} (nm)	τ_{obs} (ns)[a]	τ_{obs} (pre-exp factor)[b,c,d]	τ_{obs} (ns) (pre-exp factor)[a,c]	τ_{obs} (pre-exp factor)[b,c,d]
450	τ: 10.0	τ_1: 25 ps (0.94); τ_P: 10.2 ns (0.06)[d]	τ_1: 0.33 (0.89); τ_2: 9.01 (0.11)	τ_1: 17 ps (0.978); τ_2: 330 ps (0.007);[d] τ_P: 9 ns (0.015)[d]
500	τ: 10.7	τ_1: 17 ps (−0.40); τ_P: 10.2 ns (0.60)[d]	τ_1: 0.33 (0.84); τ_2: 9.15 (0.16)	τ_1: 9 ps (−0.310); τ_2: 330 ps (0.590);[d] τ_P: 9 ns (0.100)[d]
550	τ: 10.2	τ_1: 17 ps (−0.47); τ_P: 10.2 ns (0.53)[d]	τ_1: 0.33 (0.52); τ_2: 9.33 (0.48)	τ_1: 13 ps (−0.472); τ_2: 330 ps (0.526);[d] τ_P: 9 ns (0.002)[d]
600	τ: 10.3	τ_1: 20 ps (−0.42); τ_P: 10.2 ns (0.58)[d]	τ_1: 0.33 (−0.64); τ_2: 9.47 (0.36)	τ_1: 17 ps (−0.443); τ_2: 330 ps (−0.094);[d] τ_P: 9 ns (0.463)[d]
650	τ: 10.2	τ_1: 25 ps (−0.52); τ_P: 10.2 ns (0.48)[d]	τ_1: 0.33 (−0.62); τ_2: 9.61 (0.38)	τ_2: 330 ps (−0.460);[d] τ_P: 9 ns (0.540)[d]

[a]Lifetime was measured by using a TCSPC system with a pulsed hydrogen-filled lamp as the excitation source (λ_{ex} = 370 nm). [b]Lifetime was measured by using an up-conversion system with femtosecond excitation pulses (λ_{ex} = 370 nm). [c]Numbers in parentheses are normalized pre-exponential factors of the decay in percentage. [d]The time constant τ_P was determined from the TCSPC result and used for the fitting of up-conversion signals.

Scheme 2. Proposed Excited-State Planarization Process of DPAC-n[a]
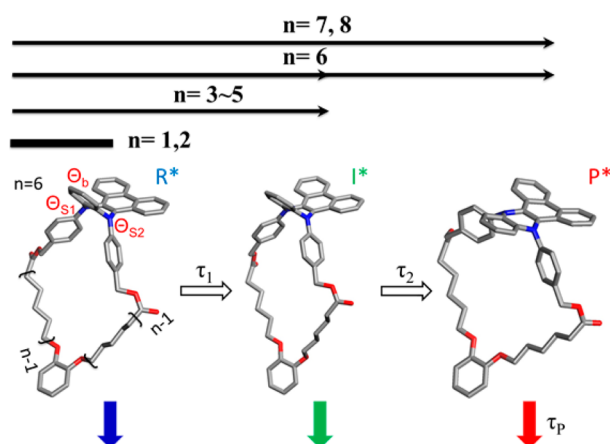
[a]For Θ_b, Θ_{S1}, and Θ_{S2}, please see Figure 1b for DPAC.

process requires a greater degree of motion, such that the strain introduced by the alkyl-ester linkage plays a more significant role (cf. R* → I* process). This viewpoint is also supported by the I* → P* process of 330 ps in **DPAC-6**, which is slower than that of 7.8 ps in **DPAC**[8a] by more than an order of magnitude. As a result, the intermediate emission **DPAC-6** in toluene can be clearly observed in a steady-state manner.

We also performed the time-resolved measurement for **DPAC-1** and **DPAC-8**. **DPAC-1** was expected to impose the largest strain, as indicated indirectly by the smallest Θ_b angle among the titled compounds (vide supra). Evidently, independent of the monitored emission wavelength (400−500 nm), solely a single emission decay of 2.0 ns was resolved, which is unambiguously ascribed to the population decay of the R* state. Apparently, the R* → I* process for **DPAC-1** is subject to the high energy barrier due to the strain imposed by the alkyl-ether chain. On the other hand, the time-resolved results shown in Figure S5 and Table S2 of SI for **DPAC-8** revealed nearly identical results with those of **DPAC**,[8a] indicating that the alkyl-ester chain of n = 8 imposes negligible strain on the overall R* → I* → P* process for **DPAC-8**.

2.4. Computational Approaches. We then developed theoretical support for the strain-imposed mechanism of this unique class of constrained V-shaped compounds. In this computational approach, we selected **DPAC-5** and **DPAC-6** as the prototypes and applied the time dependent density functional theory (TD-DFT, see SI) to access the excited-state properties, in which the $S_0 \rightarrow S_1$ absorption was calculated directly from the Franck−Condon excitation of the geometry optimized ground state. Then, the vertical $S_1 \rightarrow S_0$ transition was calculated from the structurally optimized S_1 state to obtain the emission energy gap. The calculated absorption and emission data are gathered in Table 2, including the experimental results in toluene for comparison.

For both **DPAC-5** and **DPAC-6**, as shown in Table 3, the calculated HOMOs are greatly localized in the center moiety N,N′-diphenyl-dihydropyrazine, while the LUMOs are all mainly localized at the fused phenanthrene ring. The results of computation clearly demonstrate that the lowest lying excited states for **DPAC-5** and **DPAC-6** are in part associated with the charge transfer character (Table 3). We then computed the $S_0 \rightarrow S_1$ transition for the other **DPAC-n** compounds and found that the HOMO/LUMO characters were all similar (see Tables S3 and S4 of SI), which is also the same as that of **DPAC**.[8a] This, together with the negligible contribution of the alkyl-ether or alkyl-ester chain to the frontier orbitals, rationalizes similar absorption spectra for all the studied compounds.

We also performed the calculation of dipole moment for both the ground (B3LYP/6-31+g(d,p) method) and first excited states (TD-B3LYP/6-31+g(d,p) method) based on their geometry optimized structures. As shown in Table S1, in a qualitative manner, the calculated large dipole moment for I* in the S_1 state for **DPAC-5** (22.0 D) and **DPAC-6** (24.5 D, see Table S1) versus the rather small dipole moment in S_0 (6.6 and 2.4 D for **DPAC-5** and **DPAC-6**, respectively) supports the excited-state charge transfer character. Unfortunately, the geometry optimized R* cannot be located due to the rather small R* → I* energy barrier. We also calculated the vertical electronic transition from the ground state (R), which is 384 and 390 nm for **DPAC-5** and **DPAC-6**, respectively. These values are similar to those calculated in other solvents such as in toluene (384 nm for **DPAC-5** and 390 nm for **DPAC-6**). In other words, the absorption spectrum is much less changed by the solvent polarity, reaffirming the occurrence of charge transfer in the excited state, followed by solvent relaxation and then planarization to account for the emission spectral changes.

Table 2. Experimental and Calculated Optical Characteristics for the DPAC-n Compounds[a]
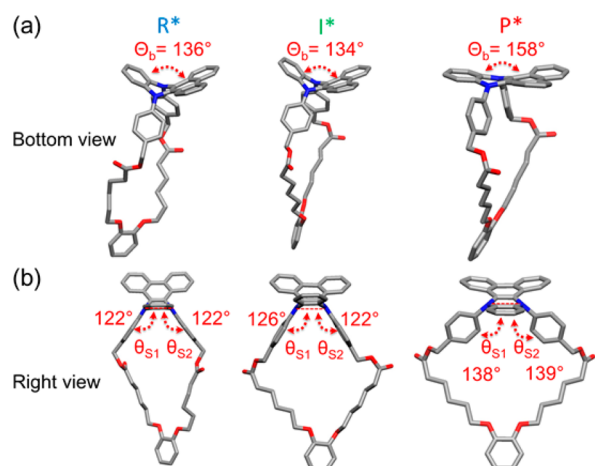
	absorption $S_0 \rightarrow S_1$			emission $S_1 \rightarrow S_0$			Stokes shift (cm^{-1})			
	λ_{exp} (nm) (ε/M^{-1} cm^{-1})	λ_{calc} (nm)	f	λ_{exp} (nm)	λ_{calc} (nm)	f	ΔE_{exp}	ΔE_{calc}	QY	τ_{obs}[b] (ns)
DPAC-1	340 (6300)	375	0.0595	400	435	0.132	4411	3678	0.20	2.01
DPAC-2	345 (8600)	380	0.093	420			5175		0.43	4.64
DPAC-3	345 (14 800)	382	0.1009	460			7246		0.59	7.53
DPAC-4	347 (11 900)	387	0.1135	478			7898		0.54	8.95
DPAC-5	347 (10 800)	384	0.1282	492	492	0.057	8493	5716	0.55	10.20
DPAC-6	350 (21 200)	390	0.1332	490	491	0.048	8163	5274	0.34	0.33, 9.01 (450 nm)
				590	543	0.068	11 622	7224		0.33, 9.61 (650 nm)
DPAC-7	350 (5000)	389	0.1406	600			11 904		0.24	8.18
DPAC-8	350 (5400)	390	0.1349	607			12 097		0.26	8.32

[a]Data were recorded in toluene at room temperature. λ_{exp} = experimental absorption/emission wavelengths, λ_{calc} = calculated absorption/emission wavelengths, ε = molar extinction coefficient, f = oscillator strengths, ΔE_{exp} = experimental Stokes shift, ΔE_{calc} = calculated Stokes shift, QY = emission quantum yield. [b]τ_{obs} = experimental emission lifetime, which is measured by the time-correlated single photon counting (TCSPC, Edinburgh FL 900) method.

Table 3. Molecular Frontier Orbitals for DPAC-5 and DPAC-6 in Their Optimized Ground-State Geometries and the Relaxed Structures in the S_1 Excited State at the Local Minima and Global Minima

	DPAC-5		DPAC-6		
Bending Angle (Θ_b)	136° (R and R*)	134° (I*)	136° (R and R*)	134° (I*)	158° (P*)
LUMO					
HOMO					

Figure 7. (a) Θ_b and (b) Θ_{S1}, Θ_{S2} of the DFT optimized geometry of **DPAC-6** in the S_1 excited state at the initially prepared state (R*), the local minimum (I*), and the global minimum (P*).

At the ground state, both geometry optimized **DPAC-5** (Figure S6) and **DPAC-6** (Figure 7) have similar Θ_b values of 136°. The optimized ground state and corresponding Franck–Condon excited state are denoted as R and R*, respectively. The vertical electronic transition from R → R* is calculated to be 384 nm for **DPAC-5** and 390 nm for **DPAC-6** in toluene (see Table 2). Note that the toluene environment was chosen because it has been widely exploited in the fluorescence up-conversion study. For **DPAC-5**, the computation result showed that, in addition to R*, there was only a global minimum in the S_1 potential energy surface (PES) located at Θ_b = 134° (see Figure S6), which is denoted as I* to correlate with the experimental result (vide supra). In stark contrast, and importantly, **DPAC-6** was found to have two energy minima, i.e., a local minimum at Θ_b = 134° denoted as I* and a global minimum at Θ_b = 158° represented as P* (Figure 7).

The vertical transition from I* → I for **DPAC-5** was calculated to be 492 nm, while the I* → I and P* → P transitions for **DPAC-6** were calculated to be 491 and 543 nm, respectively. The I* → I energy gap of ~490 nm for **DPAC-5** and **DPAC-6** matches well the steady-state intermediate emission around 490 nm (see Figure 3), while the calculated 543 nm for the P* → P transition is consistent with the onset of freely planarized emission for, e.g., **DPAC** (or **DPAC-8**) in toluene (see Figure 3).

For fair comparison, we also attempted to locate the energy minimum of any optimized structure for **DPAC-1** in the excited state and found only one global minimum in the S_1 state at Θ_b = 134°, which is the same as Θ_b = 134° for **DPAC-1** in the ground state. Therefore, we assign this state to be the optimized structure of the R* state (in S_1) reached by the Franck–Condon excitation. The estimated 435 nm emission for **DPAC-1** correlates well with its steady-state emission band maximized at 405 nm in toluene.

In addition to the difference in Θ_b among R*, I*, and P*, also noted are the changes of space/orientation on the N,N'-disubstituted side chain among the three states. For example, from an R* state at Θ_b = 136° to the local minimum I* at Θ_b = 134°, the results of calculation for **DPAC-6**, shown in Figure 7, indicate the conformational change at the N,N'-dialkoxyben-zene-alkyl-ester (or either) linkage via swinging and rotating round the N,N'-diaryls site, i.e., an increase of Θ_{S1}/Θ_{S2} from 122°/122° to 126°/122° and a decrease of $\angle$C5−C3−N1−N2 from 103° to 87°. The results indicate that **DPAC-6**, along the structural relaxation, encounters steric hindrance raised by the N,N'-disubstituted side chain. As for the I* → P* process for **DPAC-6**, in addition to the changes in Θ_b from 134° (I*) to 158° (P*), an increase of Θ_{S1}/Θ_{S2} from 126°/122° to 138°/139° and a decrease of $\angle$C5−C3−N1−N2 from 87° to 22° were also obtained. Similar structural changes of the R* → I* process were obtained for **DPAC-5**, evidenced by an increase of Θ_{S1}/Θ_{S2} from 120°/119° to 129°/127° and a decrease of $\angle$C5−C3−N1−N2 from 106° to 92° (see Figure S6).

Apparently, the dynamics of structural relaxation should be affected by the N,N'-dialkoxybenzene-alkyl-ester (or ether) linkage. Unlike with **DPAC**, in addition to the steric hindrance of N,N'-dialkoxybenzene, the structure constraint imposed by the cyclic alkyl-ester chain (Scheme 1 and Figure 2) adds an additional barrier to hinder the planarization for **DPAC-1−6** and hence results in the distinct steady-state emission spectra and the corresponding relaxation dynamics (vide supra).

Due to the structural complexity, the computational approach to assess the activation energies along R* → I* and I* → P* PES for **DPAC-6** (also, **DPAC-7** and **DPAC-8**) unfortunately failed. Experimentally, due to the use of a rotating

cell (clipped by two quartz plates) to contain the sample in the fluorescence up-conversion measurement, the temperature dependent study could not be performed. Alternatively, the much longer, subnanosecond I* → P* process (vide supra) for **DPAC-6** made possible the temperature dependent study using the TCSPC technique. Accordingly, the experiment was performed in the temperature range 283−243 K, where the viscosity of toluene varies only slightly (0.66−1.29 cP), to avoid environmental perturbation.[9] We then assumed that I* → P* is the dominant decay for I*, which follows the Arrhenius type of the thermally activated process.

$$k_{obs} = A e^{-\Delta E_a / RT}$$

Here, k_{obs} is the I* emission decay rate constant, and A and E_a denote the frequency factor and activation energy of the I* → P* planarization process. Accordingly, a logarithm of k_{obs} versus the reciprocal of absolute temperature gave a straight line, and E_a and A were calculated to be 2.3 kcal/mol and 1.59×10^{11} s^{-1}, respectively (see Figure 8). The relatively low frequency
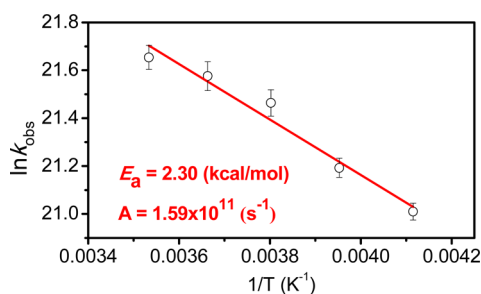
**Figure 8.** Arrhenius plot of the logarithm of rate constant (k_{obs}) versus reciprocal of the absolute temperature of **DPAC-6** in toluene from 283 to 243 K.

factor implies that the I* → P* process is associated with a large-amplitude motion, consistent with the appreciable changes of Θ_b and Θ_{S1}/Θ_{S2} calculated along the planarization process.

2.5. Ring Opening and Its Potential Application.

As opposed to the imposition of constraint by alkyl-ester linkages, releasing the structural freedom by severing the alkyl-ester linkages for **DPAC-2−6** should lead to drastic ratiometric changes of emission. We herein demonstrate a prototypical experiment for sensing triacylglycerol lipase (3.1.1.3) via its catalytic reaction to hydrolyze **DPAC-5**. Lipase is one of the most important industrial enzymes that catalyze the hydrolysis or formation of lipids. It has been extensively exploited for catalytic chiral resolution because of the growing demand for enantiopure drugs.[10] The underlying mechanism of triacylglycerol lipase catalyzed **DPAC-5** hydrolysis and the associated signal transduction are illustrated in Scheme 3a.

Theoretically, upon catalysis by lipase, the dual ester linkages of **DPAC-5** will be hydrolyzed, forming a **DPAC-OH** and a carboxylic acid (or carboxylate, depending on pH) product by rupturing the cyclic chain. Therefore, upon electronic excitation, planarization can take place for **DPAC-OH**, free from the constraint previously imposed by the alkyl-ester chain. The result should lead to drastic changes of the emission that can be exploited as an indicator of lipase activity. Experimentally, Figure 9a shows the emission spectra of **DPAC-5** in acetonitrile (ACN) and after catalysis by lipase with time in ACN:H$_2$O = 99:1 (normalized to the same

Scheme 3. (a) Proposed Hydrolyzed Reaction of DPAC-5 by Triacylglycerol Lipase (3.1.1.3) and (a + b) Overall Possible Hydrolysis Mechanism Deduced from Experimental Results
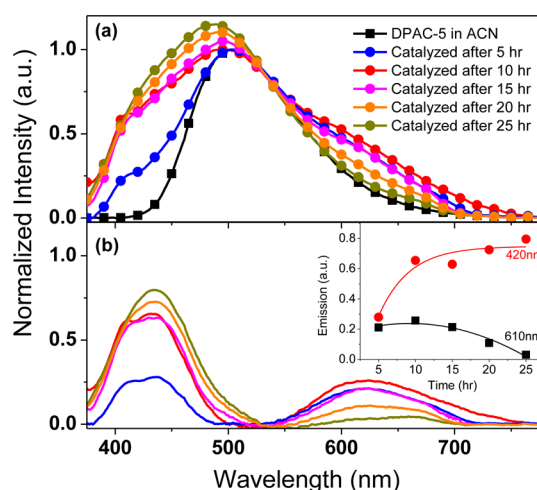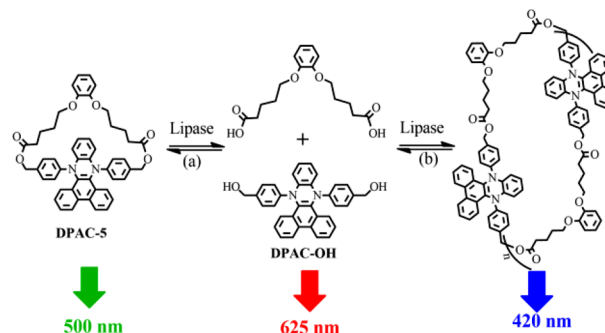
Figure 9. (a) Emission spectra of **DPAC-5** in acetonitrile (black solid square) and **DPAC-5** catalyzed by lipase with time (solid circles of various colors). (b) The difference in the emission spectra between **DPAC-5** in acetonitrile and after catalysis by lipase (λ_{ex} = 360 nm). Inset: The time dependent intensity changes of 420 and 610 nm emission bands.

intensity of **DPAC-5** (peak wavelength) in ACN). The corresponding emission changed from a single 500 nm band to multiple emission bands. We then took the difference in these two emission spectra, and the resulting spectrum is shown in Figure 9b, in which two emission band maxima at 420 and 610 nm are observed, and the time dependent intensity changes of these two emission bands are inserted in Figure 9b. While the 610 nm emission is unambiguously assigned to planarized P* emission of **DPAC-OH**, the origin of the 420 nm emission band has to be further explored. We then performed a controlled experiment by hydrolyzing **DPAC-5** in a basic aqueous solution (pH = 11), followed by extraction of the hydrolyzed products by nonpolar solvents such as toluene or hexane. Lipase was then added to the products in nonpolar solvents. Due to the presence of trace water, the Le Chatelier principle drove the reaction mainly toward esterification. The emission spectra are shown in Figures S7 and S8 of SI for *n*-hexane and toluene, respectively. Clearly, in addition to the minor 500 nm emission restored by the **DPAC-5** product, the 420 nm band is the dominant component, which may be ascribed to a cluster of esterification product from different assemblies (see Scheme 3, a+b processes). Consequently, the rigid internal environment of this cluster prohibits the structural

planarization, giving rise to the 420 nm emission (R*) from the initially prepared state.

3. CONCLUSION

In summary, we present a novel concept for modulating the excited-state process by systematically imposing various strengths of the constraint to the N,N'-disubstituted dihydrodibenzo[a,c]phenazine donor−acceptor dyads **DPAC-n** (n = 1−8), in which n correlates with the alkyl length, such that the strength of the spatial constraint decreases as n increases, in an aim to harness the conformational flexibility. Among **DPAC-n** species, the structures of **DPAC-1**, **DPAC-3**, **DPAC-4**, and **DPAC-8** were identified by X-ray crystal analysis. In stark contrast to the large Stokes-shifted 610 nm red emission for **DPAC** (absorption onset ∼400 nm), drastic chain-length n dependent emission spanning from blue (n = 1, 2, ∼400 nm) and blue-green (n = 3−5) to green-red (n = 6) and red (n = 7, 8, ∼610 nm) was observed and has been verified to originate from the charge transfer and planarization species, respectively. Scissoring the linkage releases the structural constraint and hence results in drastic changes of the emission; this approach was successfully exploited for sensing lipase activity using **DPAC-5**. The results thus demonstrate for the first time the systematic control of excited-state planarization of **DPAC-n**. On the basis of the formation and release of the constraint and hence the on and off of the planarization, future development of molecule machines driven by light may be feasible in N,N'-disubstituted dihydrodibenzo[a,c]phenazines, which deserves additional research in both fundamental studies and applications.

ASSOCIATED CONTENT

Ⓢ Supporting Information

The Supporting Information is available free of charge on the ACS Publications website at DOI: 10.1021/jacs.6b11789.

> Additional synthetic details and crystallographic, computational, and spectroscopic data along with complete references (PDF)
> Crystal data for **DPAC-1** (CIF)
> Crystal data for **DPAC-3** (CIF)
> Crystal data for **DPAC-4** (CIF)
> Crystal data for **DPAC-8** (CIF)

AUTHOR INFORMATION

Corresponding Authors

*tianhe@ecust.edu.cn
*chop@ntu.edu.tw

ORCID Ⓘ

Pi-Tai Chou: 0000-0002-8925-7747

Author Contributions

§W.C., C.-L.C., and Z.Z. made equal contributions.

Notes

The authors declare no competing financial interest.

ACKNOWLEDGMENTS

REFERENCES

(1) (a) He, G.; Guo, D.; He, C.; Zhang, X.; Zhao, X.; Duan, C. *Angew. Chem., Int. Ed.* **2009**, *48*, 6132. (b) Zhang, X.; Rehm, S.; Safont-Sempere, M. M.; Würthner, F. *Nat. Chem.* **2009**, *1*, 623. (c) Mo, H.-W.; Tsuchiya, Y.; Geng, Y.; Sagawa, T.; Kikuchi, C.; Nakanotani, H.; Ito, F.; Adachi, C. *Adv. Funct. Mater.* **2016**, *26*, 6703−6710.

(2) (a) Rotkiewicz, K.; Grellmann, K. H.; Grabowski, Z. R. *Chem. Phys. Lett.* **1973**, *19*, 315. (b) Birks, J. B. *Rep. Prog. Phys.* **1975**, *38*, 903. (c) Rettig, W. *Angew. Chem., Int. Ed. Engl.* **1986**, *25*, 971. (d) Mataga, N.; Chosrowjan, H.; Taniguchi, S. *J. Photochem. Photobiol., C* **2005**, *6*, 37. (e) Cho, D. W.; Fujitsuka, M.; Choi, K. H.; Park, M. J.; Yoon, U. C.; Majima, T. *J. Phys. Chem. B* **2006**, *110*, 4576.

(3) Grabowski, Z. R.; Rotkiewicz, K.; Rettig, W. *Chem. Rev.* **2003**, *103*, 3899.

(4) (a) Chien, Y. Y.; Wong, K. T.; Chou, P. T.; Cheng, Y. M. *Chem. Commun.* **2002**, 2874. (b) Terenziani, F.; Painelli, A.; Katan, C.; Charlot, M.; Blanchard-Desce, M. *J. Am. Chem. Soc.* **2006**, *128*, 15742. (c) Wong, K. T.; Ku, S. Y.; Cheng, Y. M.; Lin, X. Y.; Hung, Y. Y.; Pu, S. C.; Chou, P. T.; Lee, G. H.; Peng, S. M. *J. Org. Chem.* **2006**, *71*, 456. (d) Liu, C.; Tang, K. C.; Zhang, H.; Pan, H. A.; Hua, J. L.; Li, B.; Chou, P. T. *J. Phys. Chem. A* **2012**, *116*, 12339.

(5) (a) Demchenko, A. P.; Tang, K.-C.; Chou, P.-T. *Chem. Soc. Rev.* **2013**, *42*, 1379. (b) Padalkar, V. S.; Seki, S. *Chem. Soc. Rev.* **2016**, *45*, 169. (c) McDonald, L.; Wang, J.; Alexander, N.; Li, H.; Liu, T.; Pang, Y. *J. Phys. Chem. B* **2016**, *120*, 766.

(6) (a) Clegg, R. M. *Curr. Opin. Biotechnol.* **1995**, *6*, 103. (b) Jia, X.; Chen, Q.; Yang, Y.; Tang, Y.; Wang, R.; Xu, Y.; Zhu, W.; Qian, X. *J. Am. Chem. Soc.* **2016**, *138*, 10778. (c) Sasmal, D. K.; Yadav, R.; Lu, H. P. *J. Am. Chem. Soc.* **2016**, *138*, 8789.

(7) (a) Shukla, D.; Wan, P. *J. Am. Chem. Soc.* **1993**, *115*, 2990. (b) Vollmer, F.; Rettig, W.; Birckner, E. *J. Fluoresc.* **1994**, *4*, 65. (c) Doroshenko, A. O. *Theor. Exp. Chem.* **2002**, *38*, 135. (d) Chen, Y.; Zhao, J.; Guo, H.; Xie, L. *J. Org. Chem.* **2012**, *77*, 2192. (e) Yuan, C. X.; Saito, S.; Camacho, C.; Irle, S.; Hisaki, I.; Yamaguchi, S. *J. Am. Chem. Soc.* **2013**, *135*, 8842. (f) Yuan, C. X.; Saito, S.; Camacho, C.; Kowalczyk, T.; Irle, S.; Yamaguchi, S. *Chem. - Eur. J.* **2014**, *20*, 2193. (g) Saito, S.; Nobusue, S.; Tsuzaka, E.; Yuan, C.; Mori, C.; Hara, M.; Seki, T.; Camacho, C.; Irle, S.; Yamaguchi, S. *Nat. Commun.* **2016**, *7*, 12094.

(8) (a) Zhang, Z. Y.; Wu, Y. S.; Tang, K. C.; Chen, C. L.; Ho, J. W.; Su, J. H.; Tian, H.; Chou, P. T. *J. Am. Chem. Soc.* **2015**, *137*, 8509. (b) Chen, J. W.; Wu, Y. S.; Wang, X. D.; Yu, Z. Y.; Tian, H.; Yao, J. N.; Fu, H. B. *Phys. Chem. Chem. Phys.* **2015**, *17*, 27658.

(9) Assael, M. J.; Dalaouti, N. K.; Dymond, J. H. *Int. J. Thermophys.* **2000**, *21*, 291.

(10) (a) Lianghua, T.; Liming, X.; Min, S.; Huaying, G. *Appl. Biochem. Biotechnol.* **2007**, *142*, 194. (b) Kurtovic, I.; Marshall, S. N.; Zhao, X.; Simpson, B. K. *Fish Physiol. Biochem.* **2010**, *36*, 1041.